J Mater Sci: Mater Med (2014) 25:2421–2436
DOI 10.1007/s10856-014-5259-4

Growth on poly(L-lactic acid) porous scaffold preserves CD73 and CD90 immunophenotype markers of rat bone marrow mesenchymal stromal cells

Alessandra Zamparelli · Nicoletta Zini · Luca Cattini · Giulia Spaletta · Davide Dallatana · Elena Bassi · Fulvio Barbaro · Michele Iafisco · Salvatore Mosca · Annapaola Parrilli · Milena Fini · Roberto Giardino · Monica Sandri · Simone Sprio · Anna Tampieri · Nadir M. Maraldi · Roberto Toni

Received: 28 December 2013 / Accepted: 14 June 2014 / Published online: 5 July 2014

Abstract Few data are available on the effect of biomaterials on surface antigens of mammalian bone marrow-derived, adult mesenchymal stromal cells (MSCs). Since poly(L-lactic acid) or PLLA is largely used in tissue engineering of human bones, and we are developing a reverse engineering program to prototype with biomaterials the vascular architecture of bones for their bioartificial reconstruction, both in humans and animal models, we have studied the effect of porous, flat and smooth PLLA scaffolds on the immunophenotype of in vitro grown, rat MSCs in the absence of any coating, co-polymeric enrichment, and differentiation stimuli. Similar to controls on plastic, we show that our PLLA scaffold does not modify the distribution of some surface markers in rat MSCs. In particular, the maintained expression of CD73 and CD90 on two different subpopulations (small and large cells) is consistent with their adhesion to the PLLA scaffold through specialized appendages, and to their prominent content in actin. In addition, our PLLA scaffold favours retention of the intermediate filament desmin, believed a putative marker of undifferentiated state. Finally, it preserves all rat MSCs morphotypes, and allows for their survival, adhesion to the substrate, and replication. Remarkably, a subpopulation of rat MSCs grown on our PLLA scaffold exhibited formation of membrane protrusions of uncertain significance, although in a size range and morphology compatible with either motility blebs or shedding vesicles. In summary, our PLLA scaffold has no detrimental effect on a number of features of rat MSCs, primarily the expression of CD73 and CD90.

1 Introduction

A large number of studies have focused on the effect of biomaterials to induce differentiation of mammalian, bone

A. Zamparelli · D. Dallatana · E. Bassi · F. Barbaro · S. Mosca · R. Toni
Department of Biomedical, Biotechnological and Translational Sciences (S.Bi.Bi.T) - Laboratory of Regenerative Morphology and Bioartificial Structures/S.Bi.Bi.T. Museum - Section of Human Anatomy, University of Parma, Parma, Italy

A. Zamparelli · N. Zini (✉) · N. M. Maraldi
CNR - National Research Council of Italy, IGM, and SC Laboratory of Musculoskeletal Cell Biology, IOR, Bologna, Italy
e-mail: nicoletta.zini@cnr.it

L. Cattini
Laboratories of Immunorheumatology and Tissue Regeneration, and RAMSES, IOR, Bologna, Italy

G. Spaletta
Department of Mathematics, University of Bologna, Bologna, Italy

M. Iafisco · M. Sandri · S. Sprio · A. Tampieri
ISTEC - CNR, Faenza, Italy

A. Parrilli · M. Fini · R. Giardino
Laboratories of Preclinical and Surgical Studies, and Biocompatibility, Innovative Technologies, and Advanced Therapies (BITTA), Rizzoli Research Innovation Technology (RIT), IOR, Bologna, Italy

R. Toni
Division of Endocrinology Diabetes and Metabolism, Tufts Medical Center - Tufts University School of Medicine, Boston, MA, USA

marrow-derived mesenchymal stromal cells (MSCs) [1–3]. In contrast, very few data are available on the role played by either natural or synthetic bioerodible materials in directly influencing their immunophenotype, in the absence of differentiation stimuli, particularly in non human species like rats. These evidences would be of great help in establishing animal experimental models to test innovative, reverse engineering procedures for reconstruction with biomaterials of the natural vascular scaffolds of viscera, including bones, as we are currently pursuing [4–8]. In humans, collagen type I and fibronectin, alone or used to coat poly(L-lactic acid) (PLLA) porous membranes have been shown to increase CD73- and reduce CD105- and CD45-positive cells [9, 10], but no data are available on rat MSCs. Similarly, the immunocytochemical staining for CD105 in human MSCs grown on a mesh of the glycolide and L-lactide co-polymer, polyglactin coated with polydioxanone was found reduced with respect to that observed using either a porous membrane of mixed, collagen type I/III or a three-dimensional (3D) porous scaffold made with D-D-L-L-PLLA [11]. In contrast, the thermoresponsive acrylamide polymer, pNIPAm has proven to maintain the undifferentiated state of human MSCs via retention of their basic immunophenotype, independently on the duration of culture [12]. Finally, titanium dioxide and zinc oxide nanoparticles have been shown to profoundly alter the distribution of surface markers in human MSCs, primarily CD73 and CD90 [13]. Immunophenotype markers, therefore, represent early and reliable indexes of cell–biomaterial interaction in human MSCs, and might be equally exploited to analyze the behavior of rat MSCs.

Criteria for defining the undifferentiated state of MSCs greatly varies with species. In adult rats, basic steps to characterize MSCs include a number of surface antigens, among which the preservation of CD73 and CD90 are considered critical. In addition, a negligible presence of CD45 (around 10 % or less) and others cell-surface antigens have been required [14, 15], although the number of culture passages has been found critical to detect the entire immunophenotype profile [15]. In contrast, characterization of human MSCs requires more stringent antigenic criteria, not completely applicable to non human species [16, 17]. In any event, it is now clear that changes in the distribution of CD73 and CD90 may be predictive of changes in the functional state of rat MSCs.

Finally, mammalian MSCs behavior is influenced by the geometry of the growth surface [18]. In the case of PLLA and its congeners (e.g. poly-L/DL-lactide), the surface roughness, and type of porosity have been found to play a role both in human and rat MSCs [9, 19]. However, as seen in human MSCs, enrichment of PLLA with other biomaterials, including collagen and fibronectin [9], poly(ε-caprolactone) or PCL [20], and poly(lactic-*co*-glycolic) acid or PLGA [21] renders unclear the contribution of PLLA to any of the cellular parameters analyzed.

Since PLLA is a widely used biodegradable polymers in bone tissue engineering [22], we decided to investigate whether a PLLA scaffold retaining a simple surface geometry, without any coating, and presence of other biomaterials may keep unaltered the distribution of some immunophenotype markers (CD73, CD90) in rat MSCs at early passages (P2–P3), with respect to standard plastic (polystyrene).

2 Materials and methods

2.1 Animals and isolation of bone marrow-derived rat MSCs

A total of twelve 225–250 g (7–8 weeks old) Sprague–Dawley male rats (Charles River, Italy) were used as bone marrow donors. All animal studies were performed in accordance with the guidelines of the Institutional Ethical Committee for Animal Use in Research of the University of Parma, Italy. MSCs were isolated as recently reported [23], with modifications. Briefly, following euthanasia of animals with intraperitoneal pentobarbital (50 mg/kg), the femur bone marrow was collected by inserting a 18-gauge needle into the bone diaphysis and, under sterile conditions flushing it into a sterile Petri dish with D-MEM low glucose containing 10 % fetal calf serum, and an antibiotic–antimycotic combination of 100 μg/ml penicillin, 10 mg/ml streptomycin, and 25 μg/ml amphotericin B (Euroclone, Italy). This solution was used as a culture medium. Then, bone marrow mononuclear cells were isolated by gradient centrifugation on Histopaque-1077 (Sigma-Aldrich), and washed twice in culture medium, counted, and plated on a standard plastic, T25 flasks (Corning, USA) at a density of $2 \times 10^5/cm^2$. After 72 h, non-adherent cells were removed, the adherent ones (passage 0 or P0) re-seeded in a T25, and the medium replaced every 2–3 days. At 80 % confluence (i.e. subconfluence) cells were detached using trypsin 0.02 % EDTA for 1 min, splitted 1:2 (passage 1 or P1), and re-seeded. The cells were maintained in culture medium until passage 2 (P2), and used for all experiments.

2.2 Light microscopy

Morphology of rat MSCs was initially analyzed at every culture passage (P0, P1, P2) using an inverted, phase contrast light microscope (Zeiss Observer A1). Cells were always observed after the same time interval (5 and 10 days of culture), and images collected using a Zeiss digital camera (Axiocam HRc10-33), and software

(AxioVision). Part of P1 cells were re-seeded on 1.13 cm^2 glass coverslips at a density of $2 \times 10^4/cm^2$, and kept in culture up to subconfluence (P2). Then, cells were fixed with 2.5 % glutaraldehyde (GTA) in 0.1 M sodium cacodylate buffer, pH 7.4 for 1 h at room temperature (RT). Specimens were postfixed with 1 % osmium tetroxide containing 1.5 % potassium ferrocyanate (30 min at 4 °C), washed at every step, and sequentially stained with 1 % uranyl acetate (30 min at 4 °C), and 1 % tannic acid (Mallinckrodt, USA) in the dark for 30 min at RT. Samples were then dehydrated in graded series of ethanols, and embedded in Epon 812 resin. The resin was then allowed to polymerize 24 h at 60 °C. The embedded monolayers were finally sectioned on an ultramicrotome (Ultracut E, Richert-Jung). Semithin sections (0.5 μm thick) were stained with 1 % toluidine blue/sodium tetraborate decahydrate, and used for light microscopy (LM). All sections for LM were observed with a Nikon Eclipse E 600 apparatus, and images captured using a Nikon digital camera Dmx 1200, and a ACT-1 software.

2.3 Immunofluorescence and fluorescent phalloidin

For double-labeling immunofluorescence, rat MSCs grown at P2 on glass coverslips were rinsed with PBS (0.1 M, pH 7.4), and fixed with cold ethanol 70 % at 4 °C for 30 min. After extensive washing, the cells were incubated for 30 min in PBS containing 1 % bovine serum albumin at RT, to block unspecific binding. Labeling for immunophenotype markers was performed using primary monoclonal antibodies (BD Pharmingen, USA) directed against rat CD45 (1:10), CD73 (1:10), and CD90 (1:50) for 1 h at RT. After washes, cells were incubated with rabbit anti-mouse, fluorescein isothiocyanate (FITC)-conjugated secondary antibody (1:100, Dako, USA) for 1 h at RT. In a following step, cells were further washed, labeled with a rabbit polyclonal antibody recognizing the intermediate filament, desmin (1:50, Abcam, UK) for 1 h at RT, and sequentially processed with a tetramethylrhodamine isothiocyanate-conjugated (TRITC), anti-rabbit secondary antibody (1:100, Dako, USA) for 1 h at RT.

For single-labeling immunofluorescence, MSCs grown at P3 on PLLA scaffolds (see below) as described for scanning electron microscopy (SEM, see below), and immunostained using a primary antibody, either monoclonal (1:500, anti-β-actin, clone AC-15, Sigma-Aldrich) or polyclonal (1:50, anti-desmin, Abcam, UK) for 24–48 h at 4 °C. Following washes in buffer, cells were incubated with either a rabbit anti-mouse FITC-conjugated (1:100, Dako, USA) or an anti-rabbit, TRITC-conjugated (1:100, Dako, USA) antibody for 2 h at RT.

For fluorescent phalloidin, a 0.8 mM stock solution in DMSO was prepared using TRITC-coupled phalloidin (P1951, Sgma). Then, MSCs grown at P2 on glass coverslips were fixed in 4 % paraformaldehyde/PBS for 10 min at RT, rinsed in PBS, and permeabilized with 0.15 % Triton X-100 for 7 min. Finally, cells were stained with TRITC-phalloidin diluted 1:50 in PBS, and incubated for 1 h at RT.

Nuclei were counterstained with DAPI, and monolayers observed with either a Nikon Eclipse E600, or a Zeiss Axiophot. All images were captured using either a Nikon digital camera Dmx 1200, and ACT-1 software, or a Zeiss digital camera Axiocam MRc5, and Axiovision Rel 4.8 software.

2.4 Transmission and scanning electron microscopy

For transmission electron microscopy (TEM), ultrathin sections (90 nm thick) of Epon-embedded samples, including rat MSCs grown on glass coverslips, and PLLA scaffolds (see below) without cells were collected on 200-mesh nickel grids. Cell monolayers were stained with 3 % uranyl acetate and Reynold's lead citrate, whereas PLLA was kept unstained. All samples were examined with a Zeiss EM109, TEM apparatus. Images were captured using a Nikon digital camera Dmx 1200F, and ACT-1 software.

For SEM, monolayers grown at P2 on glass coverslips, and at P3 on PLLA scaffolds (see below), were fixed in GTA 2.5 % in 0.1 M sodium cacodylate buffer pH 7.4 for 1 h at RT, dehydrated in graded series of ethanols, immersed in absolute acetone (except cellular samples on PLLA scaffolds), and subjected to critical point drying. Samples of plastic (polystyrene) from culture flasks, and PLLA scaffolds without cells were quickly rinsed in absolute ethanol, and further processed without critical point drying. All samples were mounted on aluminium stubs, and metallized for 90 s using gold sputtering, to cover cells and scaffolds with a 60 nm gold film. The preparations were examined using a Philips 501 apparatus coupled to a Nikon Coolpix digital camera for acquisition of images.

2.5 Flow cytometry and immunophenotyping

Rat MSCs at P2 on either standard flasks or multiwell dishes, and on PLLA scaffolds (see below) at P3 were trypsinized, centrifuged at $220 \times g$ for 10 min, resuspended in culture medium, and counted. A solution of 7×10^4 cells in 100 μl of a PBS buffer containing 0.1 % sodium azide, and 2 % fetal bovine serum was used for each flow cytometric point. Cells were incubated at 4 °C for 15 min with monoclonal antibodies against the rat CD45, CD73, and CD90 antigens (BD Pharmingen, USA), and their isotype controls (IgG2a, Abcam, UK), all at a concentration of 1:20. Then, samples were washed with buffer, centrifuged, resuspended in the same

buffer, and incubated with FITC labeled secondary antibody (1:20, Dako, USA) for 15 min in the dark at RT. Following a final wash, the cells were analyzed using a Becton–Dickinson FACSCanto II, equipped with a blue laser capable of detecting light scatter. The FITC fluorescence was filtered by a 530 ± 21 nm bandpass filter. Two gates were applied on forward and side scatter, to select cell populations with different cell size. The frequency of positive cells was measured as the percentile of gated cells in FITC channel with activities above 99.0 % of the corresponding isotype control. The data were analyzed with FACSDIVA software (Becton–Dickinson).

2.6 Fabrication of PLLA porous scaffolds and seeding of rat MSCs on biomaterial disks

A solution of 4 % (w/v), low viscosity PLLA (Purasorb PL10 poly-L-lactide, batch n.1006000576, viscosity = 1.02 dl/g, Purac Biochem, Netherland) in methylene chloride (dichloromethane, Mw = 84.93 g/mol, n. 270997, Sigma-Aldrich) was used to prepare biomaterial scaffolds, as previously reported [8]. Specifically, 1.5 ml of polymer solution was dispensed dropwise on a glass slide previously immersed in water, to favour homogeneous layering of the polymer. Solvent volatilization was obtained under forced ventilation at RT for 4–5 min, and the resulting polymeric sheet was slashed with a sharp round punch of 10 mm in diameter, to yield porous disks of 0.785 cm^2. Disks were then sterilized by overnight incubation with an antibiotic–antimycotic solution (100 µg/ml penicillin, 10 mg/ml streptomycin, 25 µg/ml amphotericin B), followed by UV light for additional 12 h.

PLLA porous disks were placed at the bottom of 48-well plastic dishes and, to avoid scaffold floating a sterilized glass cylinder with an open surface of 0.2 cm^2 (0.5 cm internal diameter) was placed on each PLLA disk. Cells were grown on standard plastic flasks up to P2, detached, seeded on the disk surface at density of $4 \times 10^4/cm^2$, and let to replicate for 10 days (P3), with medium changes every 48 h. Control cells at identical concentration were grown for the same time directly onto plastic wells. Morphology of MSCs was studied with LM immunofluorescence, differential interference contrast Nomarsky optic, and SEM, and their immunophenotype characterized by flow cytometry.

2.7 Replication analysis

Replication efficiency and velocity of rat MSCs seeded on either plastic or PLLA disks were calculated based on a well established procedure [24]. Specifically, cells seeded at initial density (N_0) were detached at subconfluence, stained with trypan blue, and counted with a cell count chamber (N); this procedure was repeated for all passages, and cell-doubling (CD) number determined as:

$$CD = \ln(N/N_0)/\ln 2.$$

In addition, mean doubling time (DT) was estimated at each culture passage according to the following formula:

$$DT = CT/CD,$$

where CT was the cell culture time in days.

2.8 Statistical and numerical analysis

Differences in the mean number of cells at subconfluence, CD, and DT, at each culture passage on either plastic or PLLA were evaluated using a one-way analysis of variance (ANOVA), and a Student–Newman–Keuls test on means.

Differences in the number of cells positive for the various immunophenotype markers in control versus PLLA-grown rat MSCs were analyzed after arcsine transformation of their percentage values [25]. Then, each group of data was treated as a single quantitative set characterizing the stem cell immunophenotype. Comparisons between set values were performed using a one-way ANOVA.

All differences were considered significant if $P < 0.05$.

To enforce the power of prevision of the statistical evaluation on small sets of data, we performed an analysis of similarity in the distribution of cells positive for the entire set of immunophenotype markers, in controls with respect to PLLA-grown cells, using a numerical procedure based on polynomial modelling of the arcsine values. Specifically, each set of data corresponding to the entire marker distribution was interpolated using a polynomial in monic form as:

$$p(t) = a_0 \times t^0 + a_1 \times t^1 + a_2 \times t^2 + a_3 \times t^3 + a_4 \times t^4 + t^5$$

so that a companion matrix with related eigensystem was obtained [26, 27]. In this manner, it was possible to search for diagonalization of the companion matrix, and obtain specific eigenvalues, that were used to estimate departure from similarity between distributions of immunophenotype markers. Extent of departure from similarity was quantified computing numerical relative errors between couples of companion matrixes, i.e. between the distributions of the different immunophenotype data. Results were expressed using the two-norm function, chosen with the assumption of establishing the worst case distance, i.e. the widest difference between immunophenotype distributions [26, 27].

3 Results

3.1 Replication kinetic and morphology of rat MSC subtypes grown on plastic

Figure 1 shows the expansion behavior of MSCs grown on plastic dishes at passages from P0 to P2, the microscopic

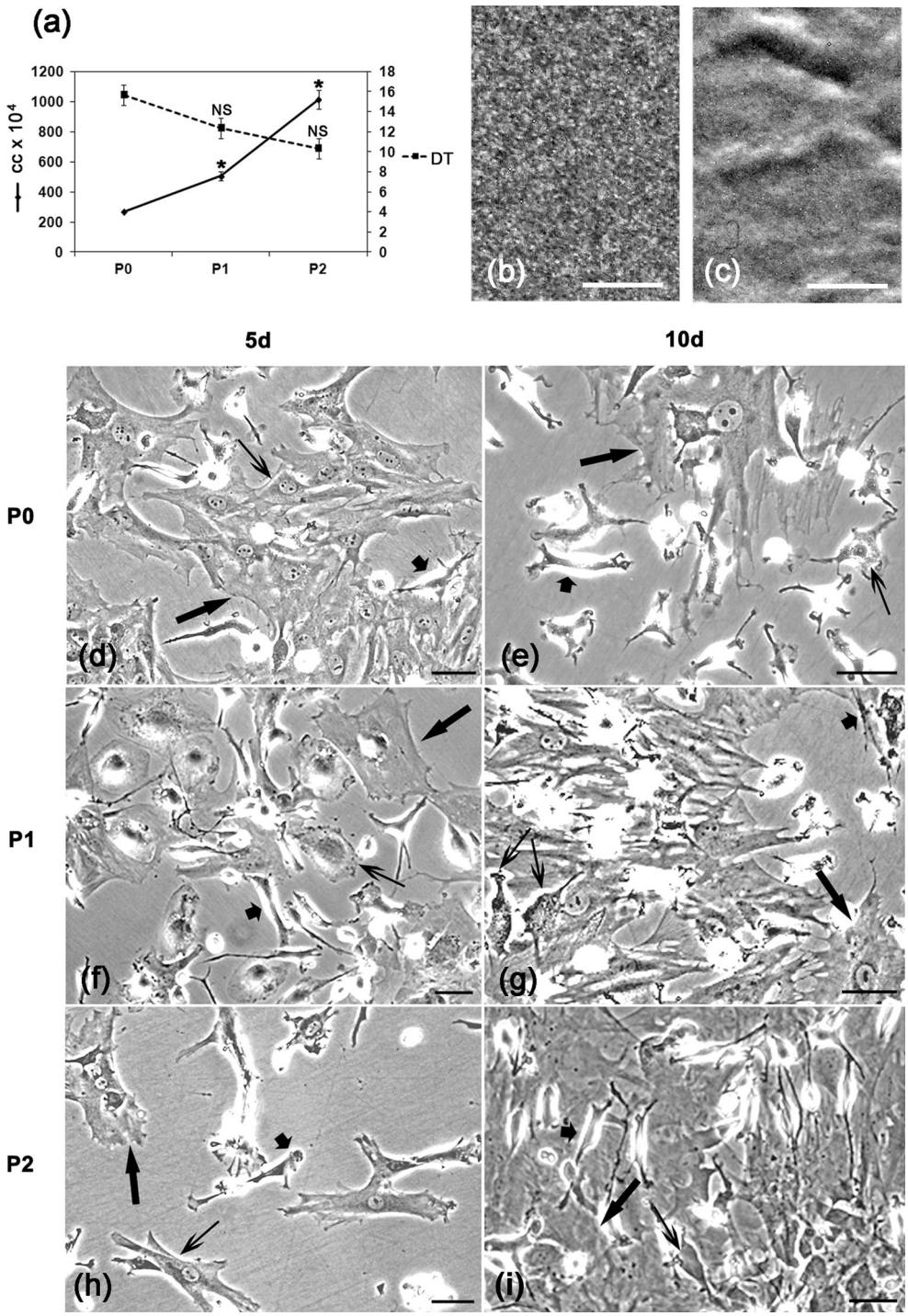

Fig. 1 Kinetic of replication of MSCs adherent to standard plastic flasks, SEM analysis of plastic (polystyrene) used to grow control MSCs, and their morphological appearance during the time of culture. **a** Mean number of cells at subconfluence, and mean DT, during all culture passages. Each point represents the mean ± SE of three separate experiments. A statistically significant increase in cell number was detected, indicating increased cell replication. In contrast, DT remained statistically unchanged, showing constancy of velocity in cell replication. **b** Surface of cell growth from a standard, polystyrene T25 flask. Note the granulosity and roughness, due to the coating material provided by the manufacturer for optimal cell attachment; **c** external surface of the same flask, showing an irregular, grooved, and bumped layer of polystyrene without any coating; **d–i** at the inverted LM, three different cell phenotypes were identified, including fibroblast-like (*short thick arrow*), polygonal (*thin arrow*), and large-flattened (*long thick arrow*) cells. These morphotypes were always detected during each of the culture passages (*P0*, *P1*, *P2*), as shown at identical time points (days 5 and 10); $*P < 0.05$; *cc* cells; *bars* in **b**, **c** 0.25 μm; *bars* in **d–i** 5 μm

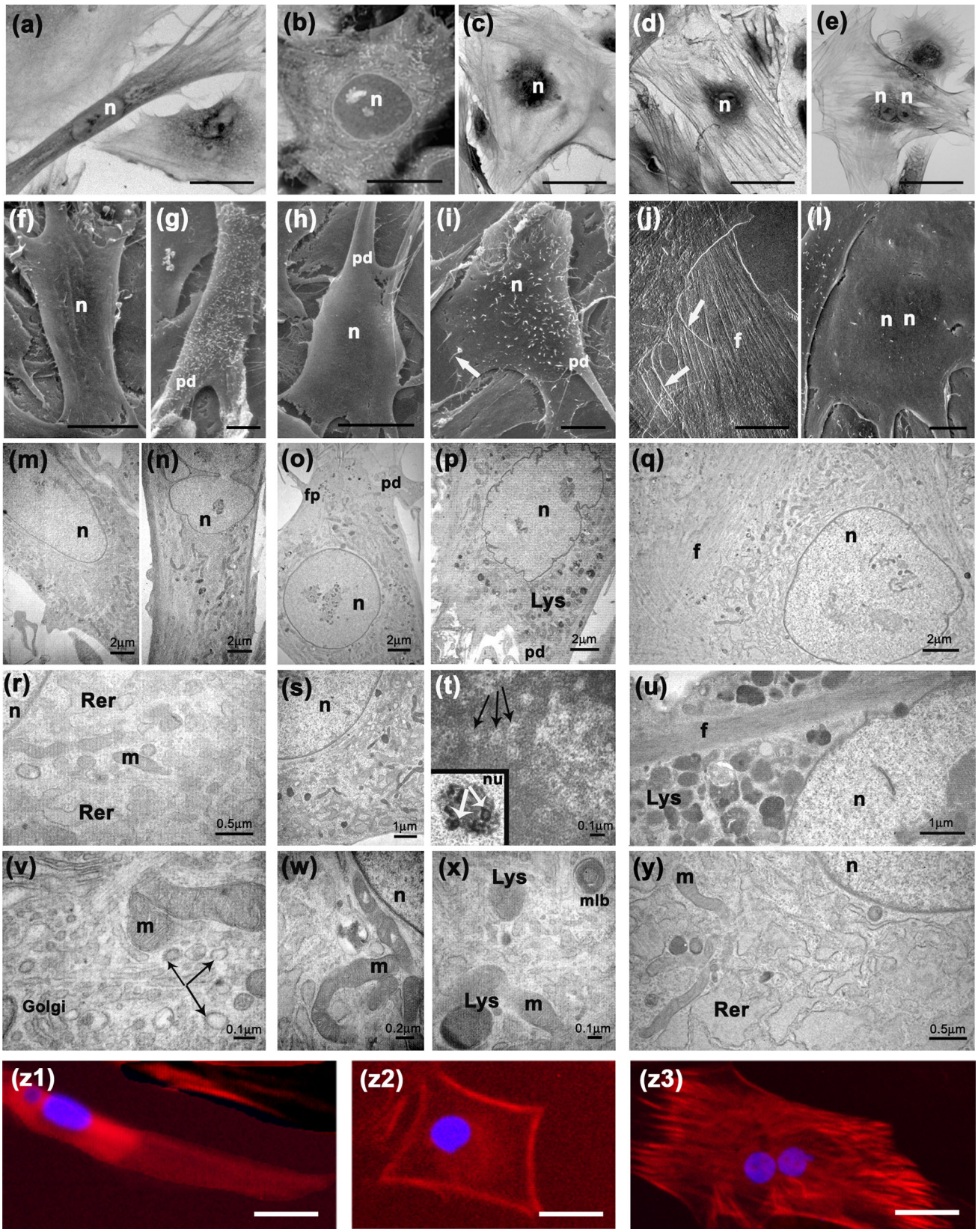
(a)
n
(b)
n
(c)
n
(d)
n
(e)
n n
(f)
n
(g)
pd
(h)
pd
n
(i)
n
pd
(j)
f
(l)
n n
(m)
n
2μm
(n)
n
2μm
(o)
fp
pd
n
2μm
(p)
n
Lys
pd
2μm
(q)
f
n
2μm
(r)
n
Rer
m
Rer
0.5μm
(s)
n
1μm
(t)
nu
0.1μm
(u)
f
Lys
n
1μm
(v)
m
Golgi
0.1μm
(w)
n
m
0.2μm
(x)
Lys
mlb
Lys
m
0.1μm
(y)
m
n
Rer
0.5μm
(z1)
(z2)
(z3)

◀**Fig. 2** Morphology, and F-actin content of control MSCs, at P2. LM appearance of **a** fibroblast-like, **b**, **c** polygonal, and **d**, **e** large-flattened MCSs. Note that all cell phenotypes contained cytoskeletal filaments, particularly dense and diffused in the large-flattened cells sometimes depicting two nuclei, as opposed to fibroblast-like and polygonal elements. SEM of **f**, **g** fibroblast-like, **h**, **i** polygonal, and **j**, **l** large-flattened MSCs. Note that both fibroblast-like and polygonal phenotypes exhibited numerous filopodia on the cell surface, as opposed to the large-flattened ones having numerous filopodia on the cell perimeter (*white thick arrows*). TEM of **m**, **n**, **r**, **v** fibroblast-like, **o**, **p**, **s**, **t**, **w**, **x** polygonal and **q**, **u**, **y** large-flattened MSCs. Note indentation of nuclei, and the diffuse distribution of subcellular organelles in both fibroblast-like and polygonal elements, as opposed to the more regular nuclear shape, and prominent perinuclear distribution of subcellular organelles in large-flattened cells. In addition, fibroblast-like cells were rich in clear vesicles (**v**, *thin arrows*), whereas polygonal cells exhibited numerous nuclear pores (**t**, *thin arrows*), and nucleoli with well developed nucleolar organizing regions (**t**, *thick white arrows* in *inset*). Finally, all cellular phenotypes shared large and elongated mitochondria, and abundant and dilated rough endoplasmic reticulum. LM staining with phalloidin revealed the presence of F-actin in all three cell morphotypes (**z1**, **z2**, **z3**), in a distribution consistent with that of microfilaments observed at TEM (**q**, **u**). Images were selected from two (LM, TEM) and three (SEM) separate experiments, after 8–19 (LM, TEM) and 10 (SEM) days of growth on glass coverslips. *f* filaments, *fp* filopodia, *Golgi* golgi apparatus, *Lys* lysosome, *m* mitochondria, *mlb* multilamellar body, *n* nucleus, *nu* nucleolus, *pd* pseudopodia, *Rer* rough endoplasmic reticulum, *bars* in **a**–**e** 5 μm, *bars* in **f**–**l** 10 μm; **z1**–**z3** 2.5 μm

geometry of the plastic (polystyrene) from standard T25 flasks used to grow control MSCs, and the morphology at the inverted LM of control MSCs for the entire period of subculture. A statistically significant increase in the mean number of cells at subconfluence was found at each passage, indicating enhanced cell replication during the subculturing procedure. In contrast, no statistically significant difference was observed in DT; therefore, it was clear that the velocity of cell replication was unchanged at each culture passage (Fig. 1a). At SEM, the plastic surface of growth was covered by a granular layer, likely corresponding to the material used by the manufacturer to provide optimal cell attachment. It appeared as an homogeneous rough surface with fine granularity (Fig. 1b). In contrast, the external flask surface resulted in an irregular, grooved and bumped layer of polystyrene devoid of any coating (Fig. 1c). At each culture passage, three different cell morphologies (morphotypes) were consistently identified, including fibroblast-like, polygonal, and large-flattened elements (Fig. 1d–i), apparently maintaining a constant proportion during each culture passage.

Figure 2 details the morphology of the three MSCs phenotypes observed in controls. In particular, fibroblast-like (Fig. 2a, f, g, m, n, r, v) and polygonal (Fig. 2b, c, h, i, o, p, s, t, w, x) cells depicted abundant filopodia on their entire surface, and cytoplasmic organelles diffused throughout the cell body. In addition, well developed clear cytoplasmic vesicles and Golgi apparatus were observed in the former cell type.

Table 1 Distribution of subcellular structures in the MSC phenotypes

Subcellular morphology	Fibroblast-like	Polygonal	Large-flattened
Nucleus	Regularly ovoidal	Regularly round	Roundish
	Irregularly invaginated	Irregularly indented	Sometimes two
	Euchromatic	Euchromatic	Euchromatic
Nucleolus	Prominent, two or more, well developed NOR	Prominent, two or more, well developed NOR	Prominent, two or more, well developed NOR
Cytoplasm	Widespread organelles	Widespread organelles	Perinuclear organelles
Rer	Abundant and dilated	Abundant and dilated	Abundant and dilated
Mitochondria	Enlarged and elongated	Enlarged and elongated	Enlarged and elongated
Lysosomes	Widespread	Widespread	Perinuclear
Multilamellar bodies	Rare	Rare	Absent
Golgi apparatus	Well developed	Some	Some
Clear cytoplasmic vesicles	Numerous	Scarce	Scarce
Filaments	Present	Present	Numerous and dense
Pseudopodia	Prominent	Prominent	Prominent
Filopodia	Numerous on the surface	Numerous on the surface	Scanty on the surface
			Numerous on the perimeter

Finally, cytoskeletal filaments resulted densely distributed at the cell periphery in both cell types. In contrast, large-flattened cells (Fig. 2d, e, j, l, q, u, y) were characterized by long peripheral filopodia, absence of multilamellar bodies, and presence of dense and parallel cytoplasmic filaments secluding subcellular organelles in perinuclear position, primarily lysosomes. However, all MSCs had large and elongated mitochondria, and abundant and dilated rough endoplasmic reticulum. In all morphotypes, staining with phalloidin (Fig. 2z1–z3) revealed presence of F-actin in a distribution recapitulating that of filaments observed by TEM. Table 1 summarizes the different subcellular features of each morphological type of rat MSCs.

3.2 Immunophenotype profile and intermediate filament content of control rat MSCs subtypes

Figure 3 highlights the behavior of the immunophenotype in MSCs grown on plastic dishes, at P2. Using flow cytometry,

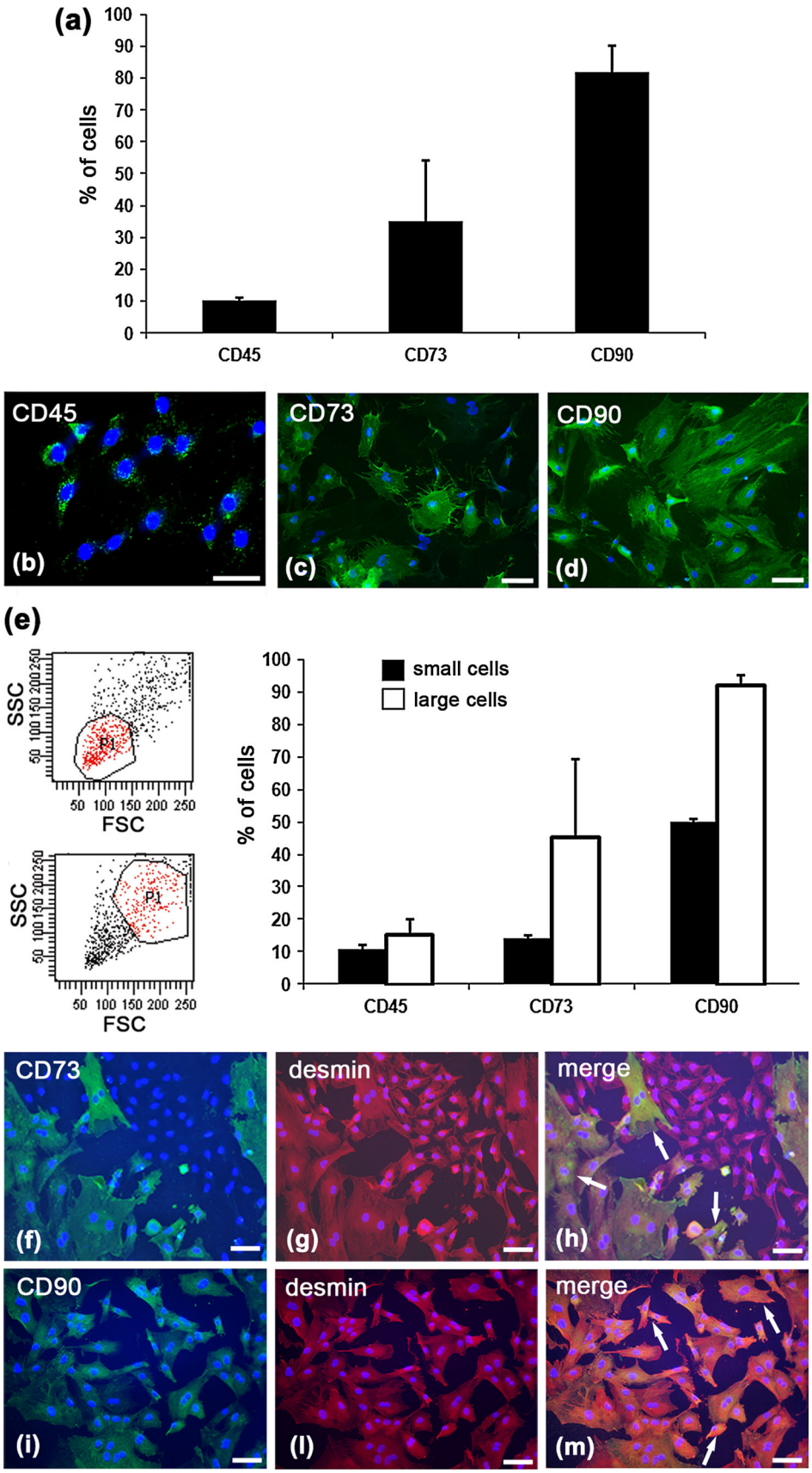

Fig. 3 Distribution and appearance of immunophenotype markers, and multipotency-related, intermediate filament desmin in control MSCs, at P2. **a** Percentage of CD45-, CD73-, and CD90-positive cells in the entire culture population grown on plastic. Each bar represents the mean ± SD of two (CD45) and three (CD73, CD90) separate experiments, as obtained by flow cytometry; **b–d** immunofluorescence of each surface marker showing its presence in progressively wider, immunopositive populations in accord with the cytometric evidence; **e** flow cytometric gating on small and large cells, and percentage of CD45-, CD73-, and CD90-positive MSCs in cellular subpopulations grown on plastic. Each bar represents the mean ± SD of two (CD45) and three (CD73, CD90) separate experiments, as obtained by flow cytometry; **f–h** double-labeling, immunofluorescence of CD73, and desmin. Note that all cell morphotypes are immunolabeled (*white arrows* in **h**); **i–m** double-labeling, immunofluorescence of CD90, and desmin. Note that all cell morphotypes are immunolabeled (*white arrows* in **m**). Immunofluorescence images were selected from a single experiment, after 19 days of cell growth on glass coverslips. *Bars* in **b–d**, **f–m** 5 μm

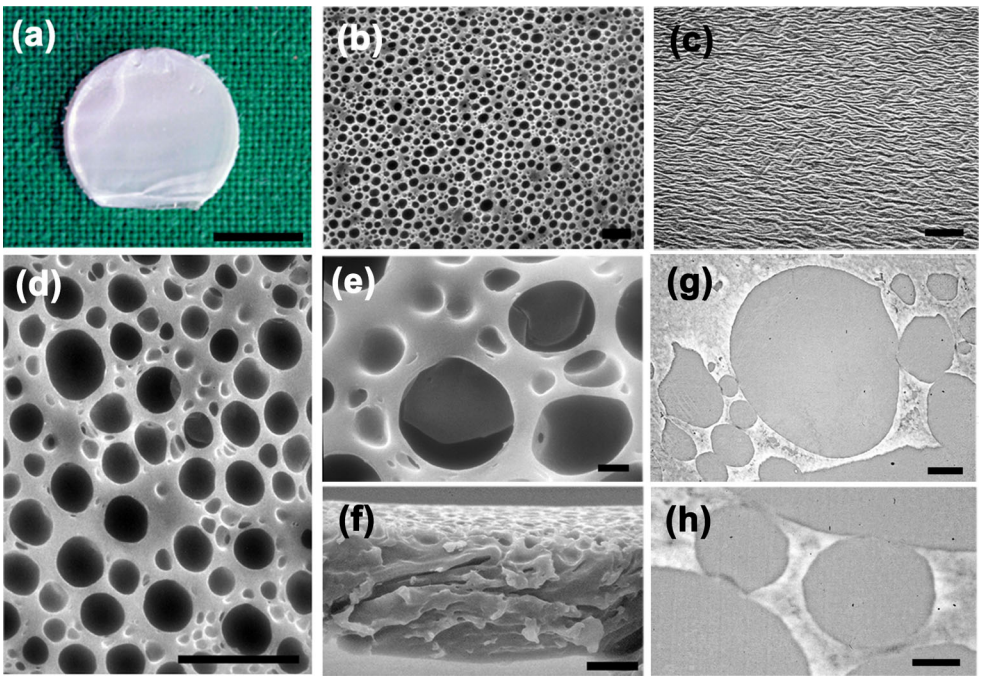

Fig. 4 Geometry of the PLLA scaffold. **a** Macroscopic geometry of the PLLA disk. It fitted the size of a single space in a 48-well culture plate; **b** appearance of the cell seeding surface of the disk, as revealed by SEM. Note the homogeneous distribution of pores, as opposed to **c** the non-seeding disk surface, constituted by a rough melt of biomaterial; **d**, **e** SEM analysis of the PLLA cell seeding surface at different magnifications, showing presence of *irregular*, *oval* and *round pores* with *closed bottom*, having a size ranging from 0.5 to 30 μm in diameter, with the majority being less than 15 μm; **f** SEM evaluation of the disk thickness, revealing a range of 10–30 μm; **g**, **h** TEM images of the *disk pores*, sectioned perpendicular to the PLLA growth surface. Note that pores had no interconnections along their cranio-caudal axis. However, in single instances pores resulted contiguous along their perimeter, without any solution of continuity. *Bars* in **a** 0.5 cm, in **b–d**, **f** 10 μm; in **e** 1 μm; in **g** 2 μm; in **h** 0.5 μm

82 ± 8 and 35 ± 19 % of cells resulted immunopositive for CD90 and CD73, respectively. In contrast, only 10 ± 1 % of cell were immunopositive for CD45 (Fig. 3a). Immunofluorescence of these markers confirmed the large prevalence of CD90-positive cells with respect to those positive for CD73 and CD45 (Fig. 3b–d). Flow cytometric gating allowed for identification of two cell subpopulations, including small and large cells. Immunophenotype markers of both subpopulations distributed similarly to those observed in the total cell population, with CD90 involving the highest percentage of both small and large elements, as opposed to CD73 and CD45 involving a progressively smaller percentage of cells (Fig. 3e). Both CD73 (Fig. 3f) and CD90 (Fig. 3i) were observed in each of the three cell morphotypes; similar, the intermediate filament, desmin (Fig. 3g, l) co-localized in the same cells (Fig. 3h, m).

3.3 PLLA scaffold geometry, cell morphology and replication kinetic, immunophenotype and microfilament/intermediate filament content of rat MSCs subtypes grown on PLLA scaffolds

Figure 4 details the structure of the PLLA porous scaffolds. Macroscopically, the PLLA surface exposed to forced air ventilation during phase separation was used to grow cells. It resulted homogeneously flat (Fig. 4a); however, SEM analysis showed that this surface was characterized by a multiporous layer (Fig. 4b), in contrast to the opposite side, constituted by a rough melt of biomaterial (Fig. 4c). The porous surface was rich in irregular, oval and round holes with closed bottom, and internal diameter ranging between 0.5 and 30 μm, with the majority being less than 15 μm (Fig. 4d, e). The PLLA scaffold showed an average thickness of 10–30 μm, and absence of pores in the depth of the biomaterial (Fig. 4f); at TEM analysis, the porous structure sectioned perpendicular to the PLLA growth surface (i.e. showing the cranio-caudal axis of pores) revealed absence of pore interconnections. Only in some instances pores resulted contiguous along their perimeter, but without any solution of continuity (Fig. 4g, h).

Figure 5 depicts the replication kinetic, distribution of microfilaments and intermediate filaments, and different morphotypes of MSCs grown for 10 days on PLLA disks (P3). No statistically significant differences were observed in CD and DT between controls on plastic and PLLA-grown MSCs (Fig. 5a). In addition, MSCs on PLLA exhibited a prominent immunofluorescence for the microfilament, β-actin in a distribution recapitulating that of both

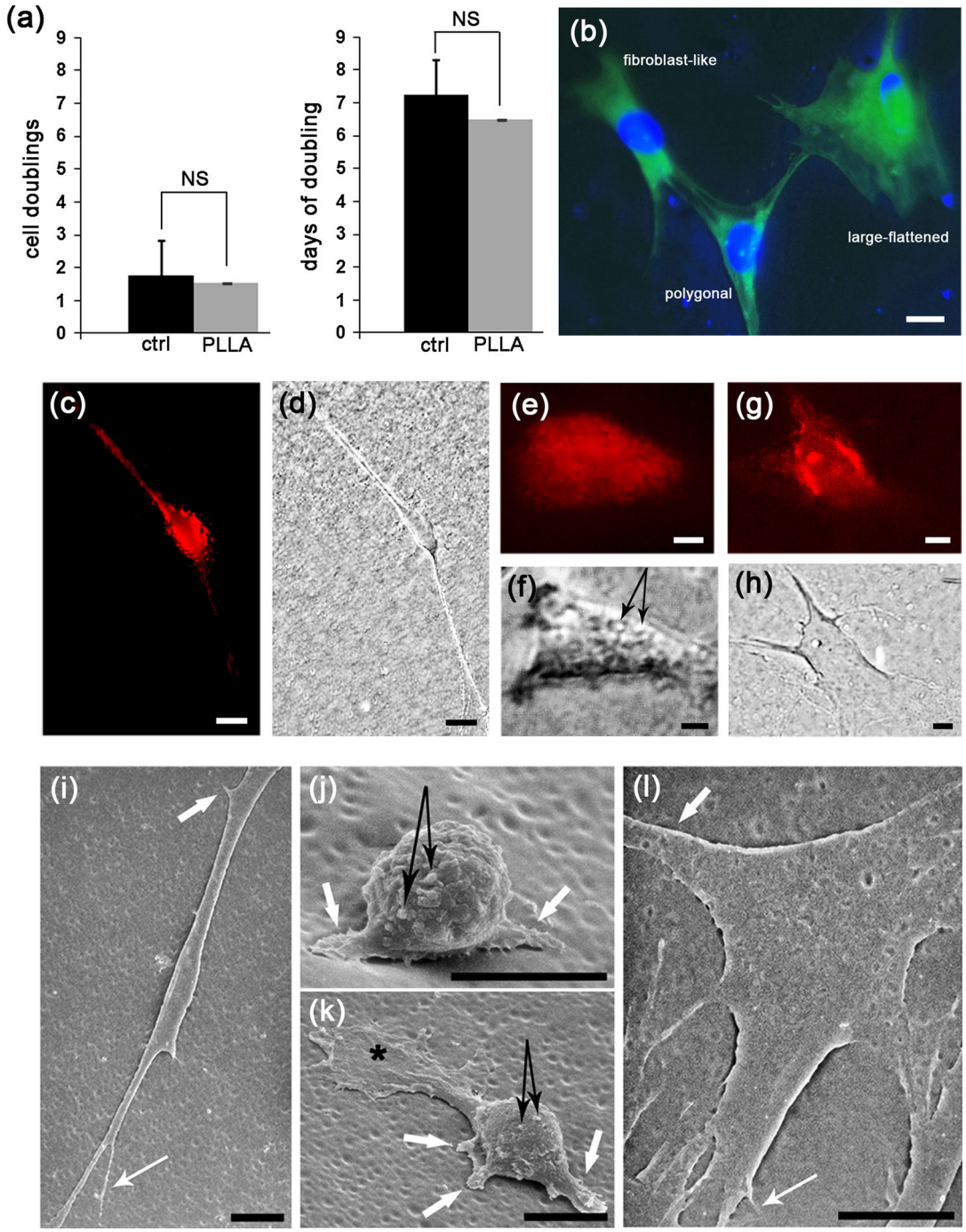

Fig. 5 Replication kinetic, cytoskeletal filament distribution, and morphology of MSCs on PLLA porous disks, at P3. **a** CD number, and mean DT after 10 days of growth on either plastic (*ctrl*) or PLLA. No statistically significant (*NS*) difference was apparent for each variable between controls on plastic and PLLA-grown cells. Each *bar* represents values of two separate experiments; **b** immunofluorescence of β-actin-labeled MSCs: all cell morphotypes previously observed on plastic were recognized; **c**, **e**, **g** immunofluorescence of desmin-labeled MSCs: all cell morphotypes previously observed on plastic were recognized; **d**, **f**, **h** differential interference contrast LM of the MSCs containing desmin. Note the consistency of these morphotypes with those described on plastic. However, polygonal elements exhibited formation of blebs on their cell surface (*long arrows* in **f**), not observed on similar and other cell types grown on plastic; **i**–**l** SEM analysis: MSCs grew in adherence on the surface of the porous PLLA disk, and depicted all the three morphologies observed in control cultures, including **i** fibroblast-like, **j**, **k** polygonal, and **l** large-flattened cells. At variance with controls, polygonal cells were characterized by numerous surface protrusions (*black arrows* in **j**, **k**) of around 700 nm in diameter, and displayed flattened and enlarged processes (*asterisk* in **k**). All phenotypes exhibited pseudopodia (*thick white* arrows in **i**–**l**) and filopodia (*thin white arrows* in **i**, **l**); *bars* in **b**–**f**, **i**–**l** 10 μm; in **g**, **h** 5 μm

thin cytoplasmic, and phalloidin-stained F-actin filaments observed by TEM and LM in control MSCs morphotypes (Fig. 5b). Similar to control MSCs, all MSCs morphotypes on PLLA were immunopositive for the intermediate filament desmin (Fig. 5c, e, g). However, polygonal cells exhibited a surface rich of protrusions (Fig. 5f) as opposed to fibroblast-like, and large-flattened cells (Fig. 5d, h) suggesting either intense cell motility or paracrine activity. At SEM analysis, all MSCs morphotypes adhered to the surface of the PLLA disk covering the pores with their soma. In addition, all three morphotypes exhibited pseudopodia and filopodia, similar to those observed in control cultures; in particular, larger processes were observed to spread and flatten onto the biomaterial (Fig. 5j–l), whereas the finest ones were sometimes seen to plunge into the depth of the PLLA holes (Fig. 5i, l). Remarkably, polygonal cells were found enriched with membrane protrusions of 670 ± 190 nm in mean diameter, thus supporting the LM finding of possible increased motility and/or paracrine secretion.

Figure 6 reports the behavior of the immunophenotype markers in control versus PLLA-grown MSCs. The percentage of MSCs positive for the immunophenotype markers, CD73 and CD90 was obtained by flow cytometry in the total cell population and, selectively in small and large cell subpopulations, at both P2 and P3. The distribution of cells positive for each of these surface markers revealed a very similar trend on plastic and PLLA, and the mean quantitative value of this distribution showed not statistically significant difference ($P > 0.05$) between experimental groups (Fig. 6a). The similarity in the quantitative behavior of cells with immunophenotype markers on plastic and and PLLA was confirmed after numerical transformation of the immunopositive cell percentages into mathematical functions (polynomials) expressing their discrete experimental values as a continuous of variations, graphically depicted by sinusoidal curves. Differences in the morphology of these curves were proven negligible by their minimal relative errors taken for the worst cases, i.e. considering the largest quantitative changes in cells positive for immunophenotype markers, either between cells on plastic or between them and those on PLLA (Fig. 6b).

4 Discussion

Reconstruction of entire, bioartificial bone segments directly on the laboratory bench (i.e. ex situ) is a recent promise of tissue engineering dependent on the availability of biocompatible materials suitable for reproduction of the 3D macro-/microscopic geometry of the native bone architecture, including its vascular channels [28, 29]. To this aim, we have recently explored innovative techniques of reverse engineering based on additive layer manufacturing to reconstruct the 3D network of vessels constituting the natural 3D scaffold of a number of soft tissue viscera [4–6]. This, with the intent to prototype with biomaterials the complex 3D vascular geometry [7, 8], primarily that of bones supposedly able to initiate recruitment and proliferation of MSCs [30], eventually leading to regeneration/reconstruction ex situ of an entire bone segment [31]. Since microporous membranes of poly(L/DL-lactide) have successfully been used to repair in vivo a number of clinically-relevant, bone defects [32] we envisaged the use of PLLA as a suitable polymer for prototyping bone vascular networks, and thus favour the expansion of MSCs, primarily in sites of complex bone healing, like nonunions [33].

To this purpose, we set an experimental model based on rat MSCs grown in adherence on a simple, thin, smooth, and microporous PLLA scaffold. Then, we analyzed whether this scaffold allowed for preservation of some immunophenotype markers, while maintaining their ability to attach to, and grow on the polymer, in the absence of differentiating factors or any other interfering substance, including biomaterial coating and/or co-polymers.

4.1 Characterization of the rat MSCs subtypes grown on standard plastic

We choose rat MSCs of a well-known strain (Sprague–Dawley) at early culture passages (P2 and P3), in light of the recent evidence that rat MSCs exhibit a morphology and proliferation potential similar to human MSCs [34], more easily replicate at low seeding density than the human counterpart [35], may quickly reach at P2–P3 a stable immunophenotype [14], and their contamination by cells with haemopoietic features (e.g. CD45-positive) quickly disappears at early steps (P2–P3), although being variably dependent on the animal strain [14, 15].

During the time-lag chosen for subculturing (P0–P2), our control monolayers on standard plastic revealed a very similar velocity in cell replication, as suggested by a not statistically significant difference in DT. However, cell replication was highly increased at later passages (P2) with respect to the earlier ones (P0, P1), as determined by a statistically significant difference in the mean number of cells at each split. In the same time interval, we consistently detected three well-characterized cell morphologies, including fibroblast-like, polygonal, and large-flattened cells. Since a higher replication potential has been observed in vitro in a subpopulation of very small, round human MSCs as opposed to spindle-like and large flat elements [36], it is be possible that also in our control system different rat cell subpopulations replicated at a variable extent.

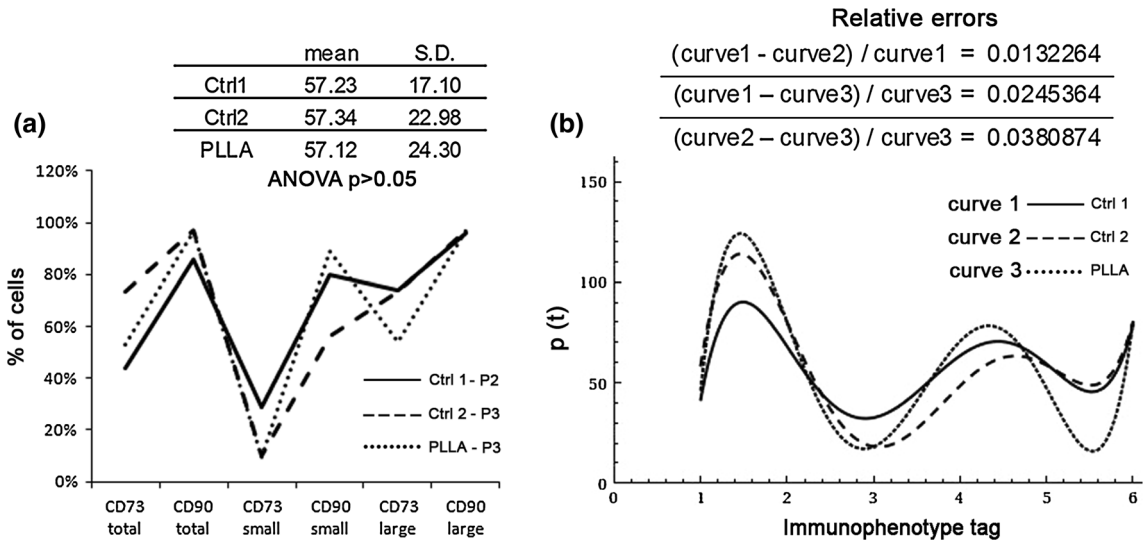

Fig. 6 Distribution of cells immunopositive for the surface markers *CD73* and *CD90*, in control versus PLLA-grown MSCs. **a** No statistically significant difference ($P > 0.05$) was observed in the mean values of each immunophenotype set (quantity of positive cells) between cells grown on plastic (controls: *1*—P2, *2*—P3) with respect to those seeded on the porous disks (PLLA, P3). Each *curve* represents a separate experiment; **b** numerical transformation of the distribution of the immunophenotype sets. Negligible differences between the number of cells grown on plastic dishes with respect to that of cells seeded on PLLA porous scaffolds were detected, as revealed by the minimal relative errors of the cases with the widest quantitative fluctuations in cells with a specific immunophenotype. The ordinate represents the value p(t) of the polynomial of cells immunolabeled for each immunophenotype marker, shown as immunophenotype tag in abscissa, in total, small, and large cells

The three observed morphotypes exhibited specific subcellular features. In particular, fibroblast-like and polygonal elements, representing cells with smaller sizes, were rich in specialized appendages (filopodia, pseudopodia) suggesting a tendency to cellular motility, adherence to the substrate, and intercellular recognition and interactions [37, 38]. Similar specializations have been previously described in rat [39, 40], and human [41, 42] MSCs. In addition, these two phenotypes showed morphological features of metabolic activity, as suggested by well developed Golgi apparatuses, and numerous intracytoplasmic clear vesicles. The latter were very different from the large, vacuolar structures described in human MSCs [36], and suggested to be dilated cysternae of the endoplasmic reticulum [39]. More likely, these vesicles are part of the endosomal traffic to and from the plasma membrane, that includes paracrine secretion of growth factors and mRNA through microvesicles (MVs), as shown in human MSCs [43]. This possibility seems confirmed by the presence in our control samples of well-developed, nucleolar organizing regions involved in ribosomal RNA synthesis, likely required to fulfill the high protein content of MVs [44].

In contrast, the large-flattened phenotype representing cells with larger sizes was featured by a segregation of subcellular organelles in perinuclear position and, similar to what described in human MSCs [36, 45], could be binucleated. Whether this phenomenon anticipates an eventual fragmentation into smaller cells, as recently described for rabbit MSCs [46], is an intriguing possibility that remains to be elucidated.

Finally, all the cell morphotypes resulted rich in F-actin filaments, as observed by fluorescent phalloidin, forming a network of parallel bundles throughout the cytoplasms. This filament pattern was confirmed by TEM, and was consistent with that recently described for F-actin in undifferentiated human MSCs [47], corroborating the appropriateness of our methodology to isolate rat MSCs. Collectively, these findings are in agreement with the evidence that in rats at least three different cell morphologies can be found at early culture phases on standard plastic, with prominence of fibroblast-like and large cells at later times [40], partly resembling phenotypes detected in human MSCs [34, 36].

4.2 Immunophenotype and intermediate filament content of rat MSCs grown on standard plastic

Our MSCs grown on plastic were analyzed by flow cytometry to determine the distribution of the surface markers CD73, CD90, and CD45. At P2, we detected presence of the surface markers CD73 and CD90 in up to 54 and 90 %, and CD45 in less than 10 % of the entire cell population, respectively. In addition, two distinct subpopulations were identified, including small and large cells, confirming the cell heterogeneity observed at LM, TEM and SEM. Both subpopulations resulted positive for the three antigens, with a prevalence of immunopositive cells in the large over the small phenotypes. Finally, both small and large cells contained a diffuse network of desmin, a contractile protein typical of differentiated smooth muscle cells, recently identified in undifferentiated

MSCs obtained by rats of the same strain and age of those used in our preparations, and believed to be a putative marker of stem cell multipotency [48].

In 2-month-old, Sprague–Dawley male rats high percentage of CD73- and CD90-positive cells (around 50 and 90 %, respectively), negligible contamination by CD45-positive elements (around 10 % or less), and cytoskeletal markers like desmin are now suggested to be typical of a stem cell phenotype [14, 15, 48]. These criteria are less restrictive than those currently applied for human MSCs, where the antigenic profile is recognized as possibly different from that of non human species [14]. Although we did not screen for a number of other surface markers of rat MSCs, nor we induced any differentiation, however the immunophenotype profile of our rat MSCs conformed to the oscillations of that reported in the strain and age of the rats we used, at the same subculture passages (P2), and was identical to that of rat MSCs exhibiting a multipotential fate [14, 15]. Therefore, we could confirm the consistency of the methodology adopted to isolate and expand rat MSCs, an inescapable step before testing on PLLA. This conclusion was reinforced by the evidence that all rat MSCs phenotypes exhibited expression of desmin, a putative marker of adult stem cells. Furthermore, identification of at least two MSCs subpopulations (small and large) was in agreement with recent data on human samples [35, 36], raising the possibility that different rat cell morphotypes have different replication and/or differentiation potentials.

4.3 Geometry of the PLLA scaffolds

We tested the effect of our PLLA scaffold on in vitro replication, morphology, microfilament and intermediate filament expression, and immunophenotype profile of the MSCs subpopulations. Our PLLA scaffold had well established geometrical features, in the absence of any biomaterial coating, and co-polymer presence. This choice was dictated by our necessity to restrict biophysical, chemical, and geometrical variables in eventual handling of the polymer for rapid prototyping of 3D vasculomorphic scaffolds, as recently investigated [4, 5, 8].

To this purpose, we prepared thin disks of biomaterial using a phase separation approach, based on solvent volatilization under forced ventilation, and we selected the layer at the biomaterial–air interface as the surface to grow cells. In this manner, we obtained a sort of membrane in a thickness range (10–30 μm) comparable to that of classical histologic sections, and we covered it with a monolayer of MSCs, to yield a pseudo-tissue slice adequate for quick processing by LM immunofluorescence, TEM, and SEM. Indeed, an approach with PLLA scaffolds made of electrospunned fibers mounted on a thermoplastic support has been recently published with similar aims, allowing for LM analysis and immunocytochemistry of the seeded cells after paraffin embedding of the entire structure [49].

Following deposition of the PLLA scaffolds at the bottom of standard plates, cells were seeded on their porous surface, and grown in static culture conditions. The PLLA disk was characterized by a mixed micro- and macro-porous surface, including holes smaller and larger than 10 μm, in a pattern similar to that recently described for 3D, PCL–PLLA porous and fibrous scaffolds with human MSCs [20]. However, in our system the size of the biomaterial holes remained limited to 10–30 μm, with the large majority being less than 15 μm in diameter, thus leading to a quasi-microporous system. In addition, analysis by TEM of pore geometry, and thickness of the PLLA disk revealed absence of any interconnection between holes, both at the level of the cell growth surface, and in the depth of the biomaterial layer. Finally, we settled a smooth growth surface, a well described PLLA modeling by liquid–liquid demixing process [50], devoid of any co-structured fibrillar organization. This, to restrain the substrate geometrical cues potentially able to alter the undifferentiated state of the MSCs through changes in elasticity/rigidity of the biomaterial [51], and thus the stem cell immunophenotype.

4.4 Effects of PLLA scaffolds on replication kinetic, cell morphology, microfilament/intermediate filament content and immunophenotype of rat MSCs

MSCs grown for 10 days on the PLLA disks revealed that cells retained their capacity to replicate. This is in agreement with previous data by Matsuzaka et al. [52], Jager et al. [11], and Eslaminejad et al. [53] who described rat and human, MSCs replication on PLLA substrates. In particular, Matsuzaka et al. [52] used rat bone marrow cells grown on a flat and either smooth or grooved, PLLA scaffolds having a biomaterial concentration very similar to our one, and groove width between 1 and 10 μm, i.e. in a size range comparable to the vast majority of our PLLA surface pores. Consistently, we did not find any variation in the replication efficiency of PLLA-grown, MSCs with respect to those seeded on standard plastic (polystyrene). Indeed, both CD and DT had no statistical significant difference with those of cells on polystyrene. However, we observed substantial geometrical differences between the surface of growth on standard polystyrene flasks and on PLLA disks. In particular, the former were characterized by a rough and granular geometry provided by a coating declared by the manufacturer as highly hydrophilic and negatively charged. In contrast, the PLLA disks depicted a flat, smooth, and non-interconnected microporous surface, supposedly hydrophobic as expected for PLLA substrates [54]. Nevertheless, our data suggest that these variables did not interfere with the replication behavior of our rat MSCs.

In addition, using a LM immunofluorescence technique based on labeling of β-actin, we observed maintenance of abundant cytoplasmic microfilaments in a bundle structure comparable to that detailed by both TEM and fluorescent phalloidin, in controls. Since it has been previously reported that actin staining in rat, bone marrow cells grown on PLLA decreases during osteogenesis [52], and PLLA per se may exert a weak osteoinductive activity when organized in a thick, 3D structure [11], but it loses this property when organized as a thin PLLA disk [52], it is possible that the maintenance of a β-actin staining pattern as that in our rat MSCs grown on a thin PLLA scaffold be compatible with a preserved undifferentiated state.

This last conclusion seems reinforced by the presence of an abundant network of intermediate filaments immunopositive for desmin, equally detectable in control MSCs grown on plastic. Since this protein has been associated to the maintenance of multipotency in rat MSCs of the same strain and age of our animals [48], it would be reasonable to expect that our PLLA scaffold did not modify this functional feature in our MSCs. However, appropriate differentiation steps are required to confirm this hypothesis. Finally, all the three cell morphotypes observed displayed specialized structures for adherence to the PLLA substrate, including pseudopodia and filopodia, similar to those detected in standard cultures on plastic, whose morphology depends on the cytoskeleton [47]. In particular, cells on PLLA covered the pores with their soma, whereas their finest appendages may sometimes penetrate the PLLA holes.

At variance with controls, however, polygonal phenotypes were found enriched with superficial protrusions in a size range of around 700 nm. Although we did not perform any specific analysis on these structures, however it is reasonable to believe that they might be either membrane blebs associated with cell motility [55, 56] or shedding MVs [44], whose involvement in cell motility is equally well known [56]. Therefore, our data raise the possibility that polygonal MSCs on our PLLA scaffold acquired either an increased motility or were stimulated to a paracrine release of biologically-active compounds, as occurring for human MSCs on congener biomaterials [11, 21, 57, 58].

Finally, we showed a similarity in the distribution of the surface markers, CD73 and CD90 between rat MSCs grown on our PLLA scaffold and plastic. To our knowledge, this is the first study reporting quantitatively, and on the basis of a statistical and numerical evaluation a direct effect of a PLLA scaffold on basic immunophenotype markers of rat MSCs, in the absence of any coating, copolymer, and differentiation stimuli. In particular, expression of CD73 has been related to increased cell motility with filopodia formation and actin accumulation in rat MSCs [59]. In contrast, it is not clear the biological meaning of CD90 in rat MSC, although it might relate to adhesion to the substrate, as in their human counterpart [17, 60]. Consistent with these antigenic activities, we detected formation of filopodia, actin accumulation, and adhesion to the substrate in our rat MSCs grown on PLLA. In addition, both surface antigens were found on small and large cells, in a proportion not different from that detected in control cultures. Taking together, these results suggest that our PLLA scaffold may act as a substrate to preserve some immunophenotype markers of adult rat, MSCs and possibly to allow for survival and expansion of cell subpopulations with different activity levels.

5 Conclusion

In summary, our data show that on in vitro conditions PLLA fabricated in a quasi-microporous, flat pattern in the absence of any coating, co-polymeric enrichment, and differentiation stimuli has no detrimental effect on a number of features in rat MSCs. In particular, our scaffold does not modify the distribution of some of their surface markers. In addition, it preserves cytoskeletal filaments including desmin, and allows for survival, replication, adhesion to the substrate, and maintenance of distinct morphotypes of rat MSCs. Finally, it induces formation of protrusions of uncertain significance on the cell membrane of a specific morphotype (polygonal cells), possibly suggesting increased cell motility or paracrine activity.

Acknowledgments The authors like to thank Daniela Galli for sound methodological advice in the preparation of MSCs, and Massimo Gamberini and Despina Kiriakidu for technical support. This work has been possible by Grants FIRB 2010 RBAP10MLK7, RBAP10KCNS, and ACPR12_00312.

References

1. Dawson E, Mapili G, Erickson K, Taqvi S, Roy K. Biomaterials for stem cell differentiation. Adv Drug Deliv Rev. 2008;60:215–28.
2. Bratt-Leal AM, Carpenedo RL, Ungrin MD, Zandstra PW, McDevitt TC. Incorporation of biomaterials in multicellular aggregates modulates pluripotent stem cell differentiation. Biomaterials. 2011;32:48–56.
3. Singh A, Elisseeff J. Biomaterials for stem cell differentiation. J Mater Chem. 2010;20:8832–47.
4. Bassoli E, Denti L, Gatto A, Paderno A, Spaletta G, Zini N, Strusi V, Dallatana D, Toni R. New approaches to prototype 3D vascular-like structures by additive layer manufacturing. In: Bartolo PJ, et al., editors. Innovative developments in virtual and physical prototyping. London: Taylor & Francis Group; 2011. p. 35–41.
5. Bassoli E, Denti L, Gatto A, Spaletta G, Paderno A, Zini N, Parrilli A, Giardino R, Strusi V, Dallatana D, Mastrogiacomo S, Zamparelli A, Iafisco M, Toni R. A combined additive layer manufacturing/indirect replication method to prototype 3D

vascular-like structures of soft tissue and endocrine organs. Virtual Phys Prototyp. 2012;7:3–11.
6. Bassoli E, Denti L, Gatto A, Spaletta G, Sofroniou M, Parrilli A, Fini M, Giardino R, Zamparelli A, Zini N, Barbaro F, Bassi E, Mosca S, Dallatana D, Toni R. A planar fractal analysis of the arterial tree of the human thyroid gland: implication for additive manufacturing of 3D ramified scaffolds. In: Bartolo PJ, et al., editors. High value manufacturing. Advanced research in virtual and rapid prototyping. London: Taylor & Francis Group; 2014. p. 423–8.
7. Toni R, Tampieri A, Zini N, Strusi V, Sandri M, Dallatana D, Spaletta G, Bassoli E, Gatto A, Ferrari A, Martin L. Ex situ bioengineering of bioartificial endocrine glands: a new frontier in regenerative medicine of soft tissue organs. Ann Anat. 2011;193:381–94.
8. Sprio S, Sandri M, Iafisco M, Panseri S, Cuhna C, Ruffini A, Zini N, Toni R, Tampieri A. Biomimetic materials in regenerative medicine. In: Ruys A, editor. Biomimetic biomaterials. Structure and applications. Cambridge: Whoodhead Publishing; 2013. p. 3–45.
9. Lee IC, Lee YT, Yu BY, Lai JY, Young TH. The behavior of mesenchymal stem cells on micropatterned PLLA membranes. J Biomed Mater Res. 2009;91:929–38.
10. Claros S, Rodriguez-Losada N, Cruz E, Guerado E, Becerra J, Andrades JA. Characterization of adult stem/progenitor cell population from bone marrow in a three-dimensional collagen gel culture system. Cell Transplant. 2012;21:2021–32.
11. Jager M, Feser T, Denck H, Krauspe R. Proliferation and osteogenic differentiation of mesenchymal stem cells cultured onto three different polymers in vitro. Ann Biomed Eng. 2005;33:1319–32.
12. Nash ME, Fan X, Carroll WM, Gorelov AV, Barry FP, Shaw G, Rochev YA. Thermoresponsive substrates used for the expansion of human mesenchymal stem cells and the preservation of immunophenotype. Stem Cell Rev. 2013;9:148–57.
13. Hackenberg S, Scherzed A, Technau A, Froelich K, Hagen R, Kleinsasser N. Functional responses of human adipose tissue-derived mesenchymal stem cells to metal oxide nanoparticles in vitro. J Biomed Nanotechnol. 2013;9:86–95.
14. Harting M, Jimenez F, Pati S, Baumgartner J, Cox C Jr. Immunophenotype characterization of rat mesenchymal stromal cells. Cytotherapy. 2008;10:243–53.
15. Barzilay R, Sadan O, Melamed E, Offen D. Comparative characterization of bone marrow-derived mesenchymal stromal cells from four different rat strains. Cytotherapy. 2009;11:435–42.
16. Dominici M, Le Blanc K, Mueller I, Slaper-Cortenbach I, Marini F, Krause D, Deans R, Keating A, Prockop DJ, Horwitz E. Minimal criteria for defining multipotent mesenchymal stromal cells. The International Society for Cellular Therapy position statement. Cytotherapy. 2006;8:315–7.
17. McNiece I. Subsets of mesenchymal stromal cells. Cytotherapy. 2007;9:301–2.
18. Martino S, D'Angelo F, Armentano I, Kenny JM, Orlacchio A. Stem cell–biomaterial interactions for regenerative medicine. Biotechnol Adv. 2012;30:338–51.
19. Gugala Z, Gogolewski S. Differentiation, growth and activity of rat bone marrow stromal cells on resorbable poly(L/DL-lactide) membranes. Biomaterials. 2004;25:2299–307.
20. Guarino V, Causa F, Taddei P, di Foggia M, Ciapetti G, Martini D, Fagnano C, Baldini N, Ambrosio L. Polylactic acid fibre-reinforced polycaprolactone scaffolds for bone tissue engineering. Biomaterials. 2008;29:3662–70.
21. Hwang NS, Varghese S, Lee HJ, Zhang Z, Elisseeff J. Biomaterials directed in vivo osteogenic differentiation of mesenchymal cells derived from human embryonic stem cells. Tissue Eng Part A. 2013;19:1723–32.
22. Meinig RP. Clinical use of resorbable polymeric membranes in the treatment of bone defects. Orthop Clin N Am. 2010;41:39–47.
23. Gao LR, Zhang NK, Bai J, Ding QA, Wang ZG, Zhu ZM, Fei YX, Yang Y, Xu RY, Chen Y. The apelin-APJ pathways exist in cardiomyogenic cells derived from mesenchymal stem cells in vitro and in vivo. Cell Transplant. 2010;19:949–58.
24. Manfrini M, Di Bona C, Canella A, Lucarelli E, Pellati A, D'Agostino A, Barbanti-Brodano G, Tognon M. Mesenchymal stem cells from patients to assay bone graft substitutes. J Cell Physiol. 2013;228:1229–37.
25. Colton T. Statistics in medicine. 13th ed. Philadelphia: Lippincott Williams & Wilkins; 1995.
26. Horn RA, Johnson CR. Matrix analysis. 1st ed. New York: Cambridge University Press; 1985.
27. Golub GH, Van Loan CF. Matrix computations. 3rd ed. Baltimore: The Johns Hopkins University Press; 1996.
28. Grayson WL, Frohlich M, Yeager K, Bhumiratana S, Chan ME, Cannizzaro C, Wan LQ, Liu XS, Guo XE, Vunjak-Novakovic G. Engineering anatomically shaped human bone grafts. Proc Natl Acad Sci USA. 2010;107:3299–304.
29. Tampieri A, Sprio S, Ruffini A, Celotti G, Lesci IG, Roveri N. From wood to bone: multi-step process to convert wood hierarchical structures into biomimetic hydroxyapatite scaffolds for bone tissue engineering. J Mater Chem. 2009;19:4973–80.
30. Murphy WL, Peters MC, Khon DH, Mooney DJ. Sustained release of vascular endothelial growth factor from mineralized poly(lactide-*co*-glycolide) scaffolds for tissue engineering. Biomaterials. 2000;21:2521–7.
31. Kaigler D, Wang Z, Horger K, Mooney DJ, Krebsbach PH. VEGF scaffolds enhance angiogenesis and bone regeneration in irradiated osseous defects. J Bone Miner Res. 2006;21:735–44.
32. Meinig RP, Rahn B, Perren SM, Gogolewski S. Bone regeneration with resorbable polymeric membranes: treatment of diaphyseal bone defects in the rabbit radius with poly(L-lactide) membrane. A pilot study. J Orthop Trauma. 1996;10:178–90.
33. Frolke JP, Patka P. Definition and classification of fracture nonunions. Injury. 2007;38S:S19–22.
34. Ayatollahi M, Salmani MK, Geramizadeh B, Tabei SZ, Soleimani M, Sanati MH. Conditions to improve expansion of human mesenchymal stem cells based on rat samples. World J Stem Cells. 2012;4:1–8.
35. Javazon EH, Colter DC, Schwarz EJ, Prockop DJ. Rat marrow stromal cells are more sensitive to plating density and expand more rapidly from single-cell-derived colonies than human marrow stromal cell. Stem Cells. 2001;19:219–25.
36. Colter DC, Sekiya I, Prockop DJ. Identification of a subpopulation of rapidly self-renewing and multipotential adult stem cells in colonies of human marrow stromal cells. Proc Natl Acad Sci USA. 2001;98:7841–5.
37. Mogilner A, Keren K. The shape of motile cells. Curr Biol. 2009;19:R762–71.
38. Wuchter P, Boda-Heggermann J, Straub BK, Grund C, Kuhn C, Krause U, Seckinge A, Peitsch WK, Spring H, Ho AD, Franke WW. Processus and recessus adhaerentes: giant adherens cell junction systems connect and attract human mesenchymal stem cells. Cell Tissues Res. 2007;328:499–514.
39. Raimondo S, Penna C, Pagliaro P, Geuna S. Morphological characterization of GFP stably transfected adult mesenchymal bone marrow stem cells. J Anat. 2006;208:3–12.
40. Karaoz E, Aksoy A, Ayhan S, Sariboyaci AE, Kaymaz F, Kasap M. Characterization of mesenchymal stem cells from rat bone marrow: ultrastructural properties, differentiation potential and immunophenotypic markers. Histochem Cell Biol. 2009;132:533–46.
41. Pasquinelli G, Tazzari R, Ricci F, Vaselli C, Buzzi M, Conte R, Orrico C, Foroni L, Stella A, Alviano F, Bagnara GP, Lucarelli E.

Ultrastructural characteristics of human mesenchymal stromal (stem) cells derived from bone marrow and term placenta. Ultrastruct Pathol. 2007;31:23–31.
42. Teti G, Cavallo C, Grigolo G, Giannini S, Facchini A, Mazzotti A, Falconi M. Ultrastructural analysis of human bone marrow mesenchymal stem cells during in vitro osteogenesis and chondrogenesis. Microsc Res Tech. 2012;75:596–604.
43. Collino F, Deregibus MC, Bruno S, Sterpone L, Aghemo G, Viltono L, Tetta C, Camussi G. Microvesicles derived from adult human bone marrow and tissue specific mesenchymal stem cells shuttle selected pattern of miRNAs. PLoS ONE. 2010;5:e11803.
44. Cocucci E, Racchetti G, Meldolesi J. Shedding microvesicles: artefacts no more. Trends Cell Biol. 2009;19:43–51.
45. Majore I, Moretti P, Hass R, Kasper C. Identification of subpopulations in mesenchymal stem cell-like cultures from human umbilical cord. Cell Commun Signal. 2009;7:6–13.
46. Ahmadbeigi N, Shafiee A, Seyedjafari E, Gheisari Y, Vassei M, Amanpour S, Amini S, Bagherizadeh I, Soleimani M. Early spontaneous immortalization and loss of plasticity of rabbit bone marrow mesenchymal stem cells. Cell Prolif. 2011;44:67–74.
47. Yourek G, Hussain MA, Mao JJ. Cytoskeletal changes of mesenchymal stem cells during differentiation. ASAIO J. 2007;53:219–28.
48. Liu Y, Deng B, Zhao Y, Xie S, Nie R. Differentiated markers in undifferentiated cells: expression of smooth muscle contractile proteins in multipotent bone marrow mesenchymal stem cells. Dev Growth Differ. 2013;55:591–605.
49. Foroni L, Dirani G, Gualandi C, Focarete ML, Pasquinelli G. Paraffin embedding allows effective analysis of proliferation, survival, and immunophenotyping of cells cultured on poly(L-lactic acid) eletrospun nanofiber scaffolds. Tissue Eng Part C. 2010;16:751–60.
50. Liu HC, Lee IC, Wang JH, Yang SH, Young TH. Preparation of PLLA membrane with different morphologies for culture of MG-63 Cells. Biomaterials. 2004;25:4047–56.
51. Engler AJ, Sen S, Sweeney HL, Discher DE. Matrix elasticity directs stem cell lineage specification. Cell. 2006;126:677–89.
52. Matsuzaka K, Walboomers F, de Ruijter A, Jansen JA. Effect of microgrooved poly-L-lactic (PLA) surfaces on proliferation, cytoskeletal organization, and mineralized matrix formation of rat bone marrow cells. Clin Oral Implants Res. 2000;11:325–33.
53. Eslaminejad MB, Bagheri F, Zandi M, Nejati E, Zomorodian E, Mivehchi H. Comparison of proliferation and osteoblast differentiation of marrow-derived mesenchymal stem cells on nano- and micro-hydroxyapatite contained composite scaffolds. Iran J Biotechnol. 2010;8:234–42.
54. Hu Y, Winn SR, Krajbich I, Hollinger JO. Porous polymer scaffolds surface-modified with arginine–glycine–aspartic acid enhance bone cell attachment and differentiation in vitro. J Biomed Mater Res A. 2003;64:583–90.
55. Paluch EK, Raz E. The role and regulation of blebs in cell migration. Curr Opin Cell Biol. 2013;25:582–90.
56. Gutwein P, Mechtersheimer S, Riedle S, Stoeck A, Gast D, Joumaa S, Zentgraf H, Fogel M, Altevogt DP. ADAM10-mediated cleavage of L1 adhesion molecule at the cell surface and in released membrane vesicles. FASEB J. 2003;17:292–4.
57. Yang ZX, Han ZB, Ji YR, Wang YW, Liang L, Chi Y, Yang SG, Li LN, Luo WF, Li JP, Chen DD, Du WJ, Cao XC, Zhuo GS, Wang T, Han ZC. CD106 identifies a subpopulation of mesenchymal stem cells with unique immunomodulatory properties. PLoS ONE. 2013;8:e59354.
58. Tiaden AN, Breiden M, Mirsaidi A, Weber FA, Bahrenberg G, Glanz S, Cinelli P, Ehrmann M, Richards PJ. Human serine protease HTRA1 positively regulates osteogenesis of human bone marrow-derived mesenchymal stem cells and mineralization of differentiating bone-forming cells through the modulation of extracellular matrix protein. Stem Cells. 2012;30:2271–82.
59. Ode A, Kopt J, Kurtz A, Shimdt-Bleek K, Schrade P, Kolar P, Buttgereit F, Lehmann K, Hutmacher DW, Duda GN, Kasper G. CD73 and CD29 concurrently mediate the mechanically induced decrease of migratory capacity of mesenchymal stromal cells. Eur Cell Mater. 2011;22:26–42.
60. Kisselbach L, Merges M, Bossie A, Boyd A. CD90 Expression on human primary cells and elimination of contaminating fibroblasts from cell cultures. Cytotechnology. 2009;59:31–44.